Thermoelectric Performance of Single-Phase Tellurium-Reduced Quaternary (PbTe)(0.55)(PbS)(0.1)(PbSe)(0.35)

SHAABANI, Laaya, BLAKE, Graeme R, MANETTAS, Andrew, KESHAVARZI, Shokat and AMINORROAYA YAMINI, Sima <http://orcid.org/0000-0002-2312-8272>

ACS OMEGA

Article

Cite This: ACS Omega 2019, 4, 9235−9240

http://pubs.acs.org/journal/acsodf

Thermoelectric Performance of Single-Phase Tellurium-Reduced Quaternary $(PbTe)_{0.55}(PbS)_{0.1}(PbSe)_{0.35}$

Laaya Shaabani,[†] Graeme R. Blake,[†] Andrew Manettas,[‡] Shokat Keshavarzi,[§] and Sima Aminorroaya Yamini*[,‡,∥]

[†]Zernike Institute for Advanced Materials, University of Groningen, Nijenborgh 4, 9747AG Groningen, The Netherlands

[‡]Australian Institute for Innovative Materials, University of Wollongong, Innovation Campus, Wollongong, 2500 New South Wales, Australia

[§]Department of Engineering, University of New Brunswick, Saint John Campus, E2L 4L5 Fredericton and Saint John, Canada

[∥]Department of Engineering and Mathematics, Sheffield Hallam University, S1 1WB Sheffield, U.K.

ABSTRACT: Lead chalcogenide quaternary systems have been shown to provide high thermoelectric (TE) efficiency superior to those of binary and ternary lead chalcogenides, arising from both altered electronic band structures and a reduction in lattice thermal conductivity. Here, we have synthesized single-phase samples of the quaternary compound $(PbTe)_{0.55}(PbS)_{0.1}(PbSe)_{0.35}$ doped with Na and characterized their TE properties. We show that the dopant solubility is limited to 1 at. %. A very low lattice thermal conductivity of ∼0.6 W m^{-1} K^{-1} at 850 K is achieved at all dopant concentrations because of phonon scattering from point defects associated with solute atoms with high contrast atomic mass. As a result, a high TE figure of merit of approximately 1.5 is achieved at 823 K in heavily doped samples. Moreover, the figure of merit is greater than 1 over a wide temperature range above 675 K.

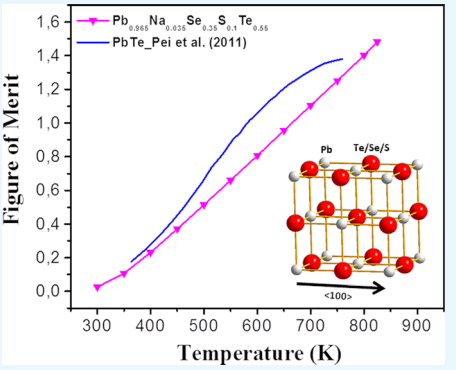

INTRODUCTION

Thermoelectric (TE) materials have attracted much research interest over the past decade, driven by the concerns arising from the energy crisis and global warming.[1] The efficiency of TE materials is generally characterized by the TE figure of merit, zT, which is defined by $zT = (S^2\sigma T)/\kappa$, where S, σ, κ, and T are the Seebeck coefficient, electrical conductivity, total thermal conductivity, and absolute temperature, respectively.[2] Some of the highest TE efficiencies at mid-range temperatures (500−900 K) have been achieved in lead chalcogenide materials[3−9] that are rich in PbTe. However, the scarcity of tellurium implies that it is essential to search for new systems comprising more earth-abundant elements that exhibit complex chemistry that can lead to high zTs.[10,11] Therefore, the focus of our research here is to identify complex lead chalcogenide systems with reduced tellurium content but without sacrificing the performance.[12−14]

Ternary systems of PbTe−PbSe[4,15,16] and PbTe−PbS[14,17−19] have been shown to exhibit higher figures of merit than binary PbQ (Q = Te, Se, and S) compounds in the temperature range of 550−800 K. The high TE performance of PbTe−PbSe alloys originates from both alteration of the electronic band structure and reduced lattice thermal conductivity due to point defects.[4,16,20] Meanwhile, the higher figures of merit achieved in PbTe−PbS alloys are attributed to a reduction in lattice thermal conductivity because of phonon scattering at the interfaces of secondary phases, as the solubility of PbS in the PbTe matrix is limited.[21] The TE performance of single-phase quaternary compounds $(PbTe)_{1-x-y}(PbS)_x(PbSe)_y$ is superior to those of both binary PbQ (Q = Te, Se, and S) and ternary PbTe−PbSe and PbTe−PbS systems,[22−26] although at low concentrations of PbS and PbSe (x and y < 0.1). This is due to enhanced Seebeck coefficients originating from a larger density of state (DOS) effective mass and band gap, as well as reduced lattice thermal conductivity due to the phonon scattering that arises from solute atoms with high contrast in atomic mass.[22,23] The presence of PbSe in quaternary compounds increases the solubility of PbS in PbTe, which results in tuning the electronic band structure,[22,23] and might also reduce the thermal conductivity further.

The quaternary samples of previous studies were all doped with Na^+ at a constant concentration, replacing 2% of Pb^{2+}.[22−25,27] Every sodium cation introduces one hole in the valence band. Sodium has been shown to be an effective dopant for Pb chalcogenides; its maximum solubility in PbS (≈2 at. %) is higher than that in PbSe (≈0.9 at. %) and much higher than that in PbTe,[28] which shows a solubility limit of ≈0.7 at. %.[29] In the present work, we have synthesized single-phase quaternary $(PbTe)_{0.55}(PbS)_{0.1}(PbSe)_{0.35}$ compounds, with a higher concentration of PbSe compared to previous reports,[22−24] at various Na dopant concentrations. The higher

Received: March 12, 2019
Accepted: April 3, 2019
Published: May 24, 2019

DOI: 10.1021/acsomega.9b00686
ACS Omega 2019, 4, 9235−9240

PbSe and PbS content increases the sodium solubility limit compared to PbTe-rich systems.[16] The band gap of the undoped compound is 0.319 eV, which is higher than those of PbTe (0.29 eV) and PbSe (0.27 eV) and lower than that of PbS (0.41 eV).[30] We find a low-lattice thermal conductivity of ~0.6 W m^{-1} K^{-1} at 850 K for all samples. Moreover, a high figure of merit of ~1.5 is achieved at 823 K in both lightly and heavily-doped samples with 55% Te on the anion site, which is higher than the maximum zT obtained for PbTe (1.4).[4]

RESULTS AND DISCUSSION

Powder X-ray diffraction (PXRD) patterns of the $Pb_{1-x}Na_xSe_{0.35}S_{0.1}Te_{0.55}$ (x = 0.01, 0.02, 0.03 and 0.035) samples are consistent with a single-phase, face-centered cubic rock salt structure (Figure 1). The refined lattice parameters

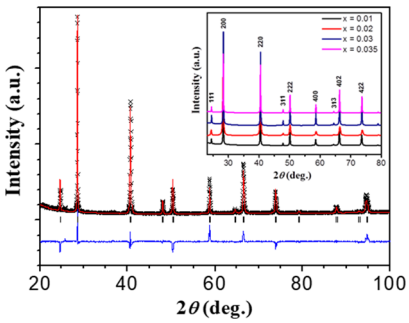

Figure 1. Observed (black data points), fitted (red line), and different (blue line) room-temperature XRD patterns of $Pb_{1-x}Na_xSe_{0.35}S_{0.1}Te_{0.55}$ (x = 0.03). The inset shows the XRD patterns of samples x = 0.01, 0.02, 0.03, and 0.035.

are 6.3020(2), 6.3111(2), 6.3002(2), and 6.2948(1) Å for the x = 0.01, 0.02, 0.03, and 0.035 samples, respectively. The lattice of these quaternary compounds contracts relative to that of pure PbTe (a = 6.46 Å) because of simultaneous alloying with PbSe (a = 6.13 Å) and PbS (a = 5.93 Å). However, there is no clear trend of a lattice parameter with Na content as the ionic radius of Na^+ (116 pm) is very close to that of Pb^{2+} (119 pm). A fit to the XRD pattern of the x = 0.03 sample is shown in Figure 1. The XRD profile is not fitted perfectly, which is mainly due to anisotropic peak broadening that is difficult to model accurately. This might reflect nanoscale defects in the underlying nanostructure.

Table 1 shows the room-temperature Hall carrier concentration and mobility for the $Pb_{1-x}Na_xSe_{0.35}S_{0.1}Te_{0.55}$ (x = 0.01, 0.02, 0.03, and 0.035) samples. The Hall coefficients, R_H, are positive for all the samples at room temperature, which indicates p-type conductivity. The Hall carrier concentration, n, and Hall mobility, μ, were obtained from the Hall coefficient measurement, using $n = 1/(eR_H)$ and $\mu = \sigma R_H$, where e is the electronic charge and σ is the electrical conductivity. The room-temperature hole carrier concentration increases from ~9.1×10^{19} cm^{-3} for the sample with x = 0.01 to ~1.7×10^{20}, 1.9×10^{20}, and ~2.3×10^{20} cm^{-3} for the samples with x = 0.02, x = 0.03, and x = 0.035, respectively. The increase in carrier concentration with dopant concentration indicates that Na^+ is incorporated into the $PbS_{0.1}Se_{0.35}Te_{0.55}$ lattice. The room-temperature Hall mobility decreases with increasing Na content, which may originate from the increased carrier concentration and consequently increased carrier scattering at dopant atoms and possibly nanoscale structural defects. The mobility of the sample with x = 0.01 is ~87 cm^2 V^{-1} s^{-1} at room temperature, which is reduced significantly for the sample with x = 0.02 (62 cm^2 V^{-1} s^{-1}). However, at concentrations above x = 0.02, the changes in carrier concentration and mobility are much smaller, which are consistent with the relatively small change in the Hall coefficient of the samples (Figure 2c).

Table 1. Hall Carrier Concentrations of $Pb_{1-x}Na_xSe_{0.35}S_{0.1}Te_{0.55}$ (x = 0.01, 0.02, 0.03, and 0.035) Samples at Room Temperature

sample	x = 0.01	x = 0.02	x = 0.03	x = 0.035
carrier concentration (cm^{-3})	9.1×10^{19}	1.7×10^{20}	1.9×10^{20}	2.3×10^{20}
mobility (cm^2 V^{-1} s^{-1})	87	62	50	42

Figure 2a,b shows the electrical resistivity (ρ) and Seebeck coefficient (S) of $Pb_{1-x}Na_xSe_{0.35}S_{0.1}Te_{0.55}$ (x = 0.01, 0.02, 0.03, and 0.035) as a function of temperature in the temperature range 300−823 K. Both ρ and S increase with temperature, indicating a typical behavior of degenerate semiconductors. The electrical resistivity decreases with Na concentration from x = 0.01 to 0.02 (Figure 2a) because of the increased carrier concentration (Figure 2c) and remains roughly the same at higher dopant concentrations. This is in agreement with the results of Table 1 and Figure 2c, which show that the carrier concentration of the samples remains roughly the same for doping levels above x = 0.02. For the x = 0.01 sample, the Seebeck coefficient (Figure 2b) increases monotonically with temperature from ~42 μV K^{-1} at 300 K to ~276 μV K^{-1} at 820 K. From 300 to 600 K, the Seebeck coefficient increases almost linearly for the heavily Na-doped samples (x > 0.01). However, at ~600 K, a change in slope is observed, which we associate with the convergence of the two valence bands. In the two valence band model, as the temperature increases, the heavy valence band merges with the light valence band and holes are transferred from the light band to the heavy band. As the DOS in the heavy band is much higher than that of the light band, a higher Seebeck coefficient is exhibited compared with that for the light band alone (given the same carrier density).[22,23,27] The contribution of the heavy band also raises the Hall coefficient of PbTe alloys at temperatures higher than 100 K (Figure 2c).[31] Therefore, the Hall coefficient of these samples should be measured at temperatures below 100 K to determine the actual carrier concentration. Although 45% of PbTe in these samples is replaced by PbSe and PbS, the temperature-dependent Hall coefficient shows a behavior typical of PbTe alloys. Figure 2d shows that sodium exhibits good dopant efficiency, allowing control of the Hall carrier concentration up to a value of 3.5×10^{20} cm^{-3} at x = 0.02 for temperatures below 100 K. The measured Hall carrier concentration [$n_H = 1/(e \cdot R_H)$] is in good agreement with the calculated carrier concentration up to x = 0.02, but deviates at higher values of x. This indicates that the successful incorporation of Na atoms in the lattice is limited to x < 0.02. Although no secondary phases appear in the XRD patterns with increasing Na concentration, suggesting that Na is entirely incorporated into the structure, excess sodium (concentrations above the solubility limit) is shown to segregate at grain boundaries and structural defects in lead chalcogenides.[32] Moreover, excess Na can form low concentrations of nanoscale

DOI: 10.1021/acsomega.9b00686
ACS Omega 2019, 4, 9235−9240

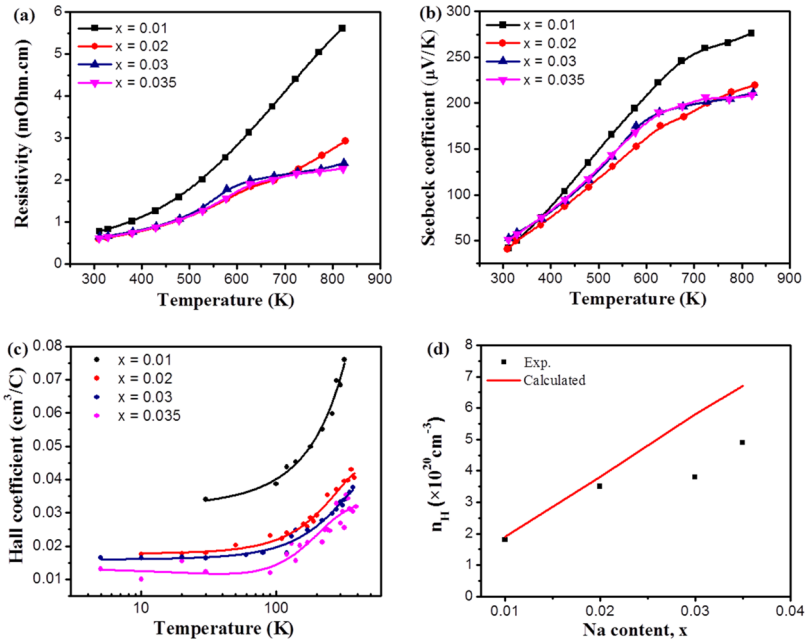

Figure 2. (a) Temperature dependence of the electrical resistivity of $Pb_{1-x}Na_xSe_{0.35}S_{0.1}Te_{0.55}$ (x = 0.01, 0.02, 0.03, and 0.035) in the temperature range 300−823 K. (b) Temperature dependence of the Seebeck coefficient of $Pb_{1-x}Na_xSe_{0.35}S_{0.1}Te_{0.55}$ (x = 0.01, 0.02, 0.03, and 0.035) in the temperature range 300−823 K. (c) Temperature dependence of the Hall coefficient below 400 K. (d) Measured Hall carrier concentration ($n_H = 1/(e{\cdot}R_H)$) below 100 K vs calculated values.

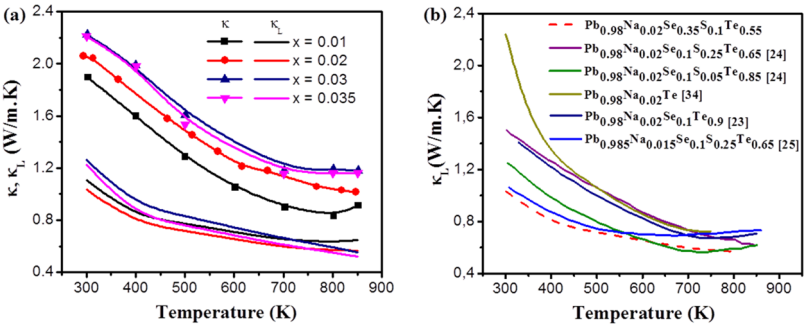

Figure 3. (a) Total thermal conductivity, κ_t, and lattice thermal conductivity, κ_L, of $Pb_{1-x}Na_xSe_{0.35}S_{0.1}Te_{0.55}$ (x = 0.01, 0.02, 0.03, and 0.035) in the temperature range 300−850 K. (b) Comparison of the lattice thermal conductivity of the x = 0.02 compound with that of the single-phase samples of Na-doped PbTe,[34] $Pb_{0.98}Na_{0.02}Se_{0.1}Te_{0.9}$,[23] and $Pb_{0.98}Na_{0.02}Se_{0.1}S_{0.05}Te_{0.85}$[24] and multiphase samples of $Pb_{0.98}Na_{0.02}Se_{0.1}S_{0.25}Te_{0.65}$[24] and $Pb_{0.985}Na_{0.015}Se_{0.1}S_{0.25}Te_{0.65}$.[25]

precipitates, which cannot be detected by XRD.[28] The Seebeck coefficient decreases with the addition of Na in $PbSe_{0.35}S_{0.1}Te_{0.55}$ over the entire 300−820 K temperature range. The most significant decrease is observed from x = 0.01 to x = 0.02, and then the variation is insignificant at higher x. This result is in agreement with the changes in carrier concentration (Figure 2d). No samples show any sign of bipolar electrical conductivity.

The total thermal conductivity, κ_{tot}, for $Pb_{1-x}Na_xSe_{0.35}S_{0.1}Te_{0.55}$ (x = 0.01, 0.02, 0.03, and 0.035) is plotted as a function of temperature in Figure 3a. The total thermal conductivity decreases with temperature for all samples and increases with dopant concentration (the total thermal conductivity of the x = 0.035 sample is roughly equal to that of the x = 0.03 sample). This is due to the significant contribution of the electronic thermal conductivity in these compounds. The thermal conductivity at 850 K for the x = 0.01, 0.02, and 0.03 samples reaches ∼0.9, 1.0, and 1.2 W m^{-1} K^{-1}, respectively. The lattice thermal conductivity, κ_L, was calculated by subtracting the electronic contribution, κ_e, from the measured total thermal conductivity such that $\kappa_L = \kappa_{total} - \kappa_e$, where the value of κ_e can be calculated by employing the Wiedemann−Franz relation, $\kappa_e = L\sigma T$, where σ is the electrical conductivity, T is the temperature, and L is the Lorenz number. An estimation of the Lorenz number as a function of temperature is made by assuming a parabolic band with acoustic phonon scattering through the equation[33]

$$L = \left(\frac{k}{e}\right)^2 \frac{3F_{0(\eta)}F_{2(\eta)} - 4F_1(\eta)^2}{F_0(\eta)^2}$$

where η is the reduced chemical potential calculated from the temperature-dependent Seebeck coefficient using the equation

$$S = \frac{k}{e}\left(\frac{2F_1(\eta)}{F_0(\eta)} - \eta\right)$$

with the Fermi integrals, $F_j(\eta)$, defined as

DOI: 10.1021/acsomega.9b00686
ACS Omega 2019, 4, 9235−9240

$$F_j(\eta) = \int_0^\infty f\varepsilon^j \, d\varepsilon = \int_0^\infty \frac{\varepsilon^j \, d\varepsilon}{1 + \exp(\varepsilon - \eta)}$$

where ε is the reduced carrier energy.

A low lattice thermal conductivity of between 1.0 and 1.3 W m^{-1} K^{-1} is obtained for all samples at room temperature, with no obvious dependence on doping concentration. This implies that the extra point defects created by the dopant do not affect the degree of phonon scattering. The lattice thermal conductivity at 850 K reaches approximately 0.6 W m^{-1} K^{-1} for all samples. The lattice thermal conductivity of the sample with $x = 0.02$ is compared to that of single-phase samples of $Pb_{0.98}Na_{0.02}Te$,[3,4] $Pb_{0.98}Na_{0.02}Se_{0.1}Te_{0.9}$,[2,3] $Pb_{0.98}Na_{0.02}Se_{0.1}S_{0.05}Te_{0.85}$,[24] and multiphase samples of $Pb_{0.98}Na_{0.02}Se_{0.1}S_{0.25}Te_{0.65}$[24] and $Pb_{0.985}Na_{0.015}Se_{0.1}S_{0.25}Te_{0.65}$[25] in Figure 3b. The current samples exhibit lower κ_{latt} than the single-phase Na-doped compounds $(PbTe)_{0.65}(PbS)_{0.25}(PbSe)_{0.1}$[24] and $(PbTe)_{0.9}(PbSe)_{0.1}$,[23] as well as Na-doped PbTe below 600 K,[34] and κ_{latt} of our samples is comparable to that of the multiphase nanostructured compound $Pb_{0.985}Na_{0.015}Se_{0.1}S_{0.25}Te_{0.65}$[25] and the single-phase compound $Pb_{0.98}Na_{0.02}Se_{0.1}S_{0.05}Te_{0.85}$.[24] The microscopy analysis of single-phase polycrystalline Pb chalcogenides (with similar composition to those in the current study) shows no significant microstructural changes with slight compositional variations;[35] thus, the significantly reduced κ_{latt} in our single-phase compound can be attributed to enhanced phonon scattering arising from randomly distributed Se and S solute atoms in the matrix.

The TE figures of merit of all the samples are compared with p-type PbTe,[34] PbSe,[13] and PbS[36] as a function of temperature in Figure 4. The maximum figure of merit of ~1.5 is obtained

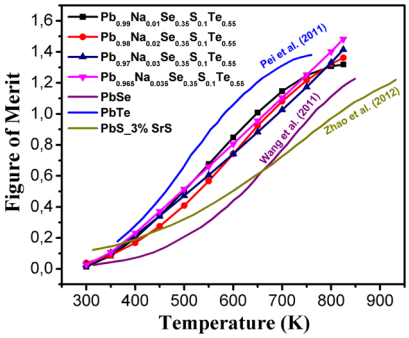

Figure 4. Temperature dependence of the TE figure of merit, zT, for $Pb_{1-x}Na_xSe_{0.35}S_{0.1}Te_{0.55}$ (x = 0.01, 0.02, 0.03, and 0.035) in the temperature range 300−823 K, compared with maximum reported zT values for binary p-type PbSe,[13] p-type Strontium-added PbS,[36] and p-type PbTe.[34]

at 823 K for the heavily doped samples. All four compounds show figures of merit of >1 over a wide temperature range above 675 K. By comparison, the figure of merit reaches 1 only above 750 K for p-type PbSe[13] and 800 K for p-type PbS.[36] The higher figure of merit obtained at lower temperatures can improve the power generation efficiency of TE devices.

CONCLUSIONS

In conclusion, we have synthesized p-type single-phase quaternary lead chalcogenide compounds in which 45% of the tellurium is substituted by more abundant elements, such as sulfur and selenium, and we have investigated the effect of various Na-dopant concentrations on the TE performance of this compound. The quaternary, single-phase Na-doped compound $(PbTe)_{0.55}(PbS)_{0.1}(PbSe)_{0.35}$ exhibits a zT of approximately 1.5 at 823 K and is above 1.0 over a wide temperature range above 675 K. The high TE performance is attributed largely to a low lattice thermal conductivity that is of comparable magnitude to multiphase nanostructured lead chalcogenides. This is due to the phonon scattering that takes place at point defects associated with solute atoms with a large atomic mass contrast.

EXPERIMENTAL SECTION

Sample Fabrication. *Synthesis.* A polycrystalline ingot of PbS was synthesized by mixing a stoichiometric ratio of high purity Pb granules (99.999%, Alfa Aesar) and S powder (99.999%, Alfa Aesar) in a vacuum-sealed quartz ampoule, followed by reacting them at 1373 K to produce a high-purity PbS starting material. Polycrystalline ingots of $Pb_{1-x}Na_xSe_{0.35}S_{0.1}Te_{0.55}$ with x = 0.01, 0.02, 0.03, and 0.035 were prepared by mixing appropriate quantities of the PbS precursor, Pb, Se granules (99.999%, Alfa Aesar), Te powder (99.999%, Alfa Aesar), and crushed Na chunks (99%, Aldrich) as the dopant, with a total mass of 10 g for each sample, loaded into carbon-coated quartz ampoules. The ampoules were sealed under vacuum, then heated to 1373 K, and held at the same temperature for 10 h. The ampoules were then quenched in cold water and annealed at 823 K for 72 h.

Sintering. The ingots obtained from the synthesis procedure mentioned above were ground by hand to a fine powder using an agate mortar and pestle and sintered into 12 mm diameter and 2 mm thickness disk-shaped pellets using spark plasma sintering (SPS) under vacuum at 793 K and an axial pressure of 40 MPa for 30 min.

Transport Property Measurements. *Seebeck Coefficient and Resistivity Measurements.* The electrical conductivity (σ) and Seebeck coefficient (S) were simultaneously measured using a Linseis LSR-3 instrument. Measurements were performed under helium atmosphere from room temperature to 823 K. The disk-shaped samples from SPS were cut and polished into parallelepiped shapes for these measurements.

Thermal Conductivity Measurements. The total thermal conductivity (κ) was calculated using the formula $\kappa = \rho D C_p$. The laser flash diffusivity method (Linseis LFA 1000) was used to measure the thermal diffusivity, D, in the temperature range 300−850 K. The density (ρ) of the sintered samples was calculated by measuring the mass and dimensions. All samples had measured densities higher than 95% of their theoretical values. The specific heat capacity (C_p) was calculated using the equation C_p (k_B per atom) = $(3.07 + 4.7 \times 10^{-4}(T/K - 300))$.[37]

Hall Measurements. Hall coefficients (R_H) were measured using a quantum design physical property measurement system under magnetic fields of up to ±2 T in the range 5−400 K.

Materials Characterization. *X-ray Diffraction.* PXRD was carried out using a GBC Scientific X-ray diffractometer operating with Cu Kα radiation (λ = 1.542 Å, 40 kV, 25 mA) at room temperature. The XRD patterns were fitted by the Rietveld method using the GSAS software suite.[38]

AUTHOR INFORMATION

Corresponding Author

*E-mail: S.Aminorroaya@shu.ac.uk.

DOI: 10.1021/acsomega.9b00686
ACS Omega 2019, 4, 9235−9240

ORCID

Graeme R. Blake: 0000-0001-9531-7649

Sima Aminorroaya Yamini: 0000-0002-2312-8272

Notes

The authors declare no competing financial interest.

■ ACKNOWLEDGMENTS

This research has been conducted with the support of an Australian Research Council Discovery Early Career Award (DE130100310). Work at the University of Groningen was supported by a Dieptestrategie grant from the Zernike Institute for Advanced Materials.

■ REFERENCES

(1) Bell, L. E. Cooling, Heating, Generating Power, and Recovering Waste Heat with Thermoelectric Systems. *Science* **2008**, *321*, 1457−1461.

(2) Goldsmid, H. J. Conversion efficiency and figure-of-merit. In *CRC Handbook of Thermoelectrics*; Rowe, D. M., Ed.; CRC Press: Boca Raton, 1995; pp 19−26.

(3) Heremans, J. P.; Jovovic, V.; Toberer, E. S.; Saramat, A.; Kurosaki, K.; Charoenphakdee, A.; Yamanaka, S.; Snyder, G. J. Enhancement of Thermoelectric Efficiency in PbTe by Distortion of the Electronic Density of States. *Science* **2008**, *321*, 554−557.

(4) Pei, Y.; Shi, X.; LaLonde, A.; Wang, H.; Chen, L.; Snyder, G. J. Convergence of Electronic Bands for High Performance Bulk Thermoelectrics. *Nature* **2011**, *473*, 66−69.

(5) Biswas, K.; He, J.; Zhang, Q.; Wang, G.; Uher, C.; Dravid, V. P.; Kanatzidis, M. G. Strained Endotaxial Nanostructures with High Thermoelectric Figure of Merit. *Nat. Chem.* **2011**, *3*, 160−166.

(6) Shi, X.; Yang, J.; Bai, S.; Yang, J.; Wang, H.; Chi, M.; Salvador, J. R.; Zhang, W.; Chen, L.; Wong-Ng, W. On the Design of High-Efficiency Thermoelectric Clathrates through a Systematic Cross-Substitution of Framework Elements. *Adv. Funct. Mater.* **2010**, *20*, 755−763.

(7) Shi, X.; Yang, J.; Salvador, J. R.; Chi, M.; Cho, J. Y.; Wang, H.; Bai, S.; Yang, J.; Zhang, W.; Chen, L. Multiple-filled Skutterudites: High Thermoelectric Figure of Merit through Separately Optimizing Electrical and Thermal Transports. *J. Am. Chem. Soc.* **2011**, *133*, 7837−7846.

(8) Bozin, E. S.; Malliakas, C. D.; Souvatzis, P.; Proffen, T.; Spaldin, N. A.; Kanatzidis, M. G.; Billinge, S. J. L. Entropically Stabilized Local Dipole Formation in Lead Chalcogenides. *Science* **2010**, *330*, 1660−1663.

(9) Biswas, K.; He, J.; Blum, I. D.; Wu, C.-I.; Hogan, T. P.; Seidman, D. N.; Dravid, V. P.; Kanatzidis, M. G. High-performance Bulk Thermoelectrics with All-Scale Hierarchical Architectures. *Nature* **2012**, *489*, 414−418.

(10) Ohno, S.; Aydemir, U.; Amsler, M.; Pöhls, J.-H.; Chanakian, S.; Zevalkink, A.; White, M. A.; Bux, S. K.; Wolverton, C.; Snyder, G. J. Achieving zT > 1 in Inexpensive Zintl Phase $Ca_9Zn_{4+x}Sb_9$ by Phase Boundary Mapping. *Adv. Funct. Mater.* **2017**, *27*, 1606361.

(11) Hsu, K. F.; Loo, S.; Guo, F.; Chen, W.; Dyck, J. S.; Uher, C.; Hogan, T.; Polychroniadis, E. K.; Kanatzidis, M. G. Cubic $AgPb_mSbTe_{2+m}$:Bulk Thermoelectric Materials with High Figure of Merit. *Science* **2004**, *303*, 818−821.

(12) Androulakis, J.; Yeseul, L.; Todorov, I.; Chung, D. Y.; Kanatzids, M. G. High-Temperature Thermoelectric Properties of n-Type PbSe Doped with Ga, In, and Pb. *Phys. Rev. B* **2011**, *83*, 195209.

(13) Wang, H.; Pei, Y.; Lalonde, A. D.; Snyder, G. J. Heavily Doped p-Type PbSe with High Thermoelectric Performance: An Alternative for PbTe. *Adv. Mater.* **2011**, *23*, 1366−1370.

(14) Johnsen, S.; He, J.; Androulakis, J.; Dravid, V. P.; Todorov, I.; Chung, D. Y.; Kanatzidis, M. G. Nanostructures Boost the Thermoelectric Performance of PbS. *J. Am. Chem. Soc.* **2011**, *133*, 3460−3470.

(15) Zhang, Q.; Cao, F.; Liu, W.; Lukas, K.; Yu, B.; Chen, S.; Opeil, C.; Broido, D.; Chen, G.; Ren, Z. Heavy Doping and Band Engineering by Potassium to Improve the Thermoelectric Figure of Merit in p-Type PbTe, PbSe, and PbTe1-ySey. *J. Am. Chem. Soc.* **2012**, *134*, 10031−10038.

(16) Kudman, I. Thermoelectric Properties of p-type PbTe-PbSe Alloys. *J. Mater. Sci.* **1972**, *7*, 1027−1029.

(17) Girard, S. N.; He, J.; Zhou, X.; Shoemaker, D.; Jaworski, C. M.; Uher, C.; Dravid, V. P.; Heremans, J. P.; Kanatzidis, M. G. High Performance Na-doped PbTe-PbS Thermoelectric Materials: Electronic Density of States Modification and Shape-Controlled Nanostructures. *J. Am. Chem. Soc.* **2011**, *133*, 16588−16597.

(18) Girard, S. N.; He, J.; Li, C.; Moses, S.; Wang, G.; Uher, C.; Dravid, V. P.; Kanatzidis, M. G. In Situ Nanostructure Generation and Evolution within a Bulk Thermoelectric Material to Reduce Lattice Thermal Conductivity. *Nano Lett.* **2010**, *10*, 2825−2831.

(19) He, J.; Girard, S. N.; Kanatzidis, M. G.; Dravid, V. P. Microstructure-Lattice Thermal Conductivity Correlation in Nanostructured $PbTe_{0.7}S_{0.3}$ Thermoelectric Materials. *Adv. Funct. Mater.* **2010**, *20*, 764−772.

(20) Heremans, J. P.; Wiendlocha, B.; Chamoire, A. M. Resonant Levels in Bulk Thermoelectric Semiconductors. *Energy Environ. Sci.* **2012**, *5*, 5510−5530.

(21) Girard, S. N.; Schmidt-Rohr, K.; Chasapis, T. C.; Hatzikraniotis, E.; Njegic, B.; Levin, E. M.; Rawal, A.; Paraskevopoulos, K. M.; Kanatzidis, M. G. Analysis of Phase Separation in High Performance PbTe-PbS Thermoelectric Materials. *Adv. Funct. Mater.* **2013**, *23*, 747−757.

(22) Korkosz, R. J.; Chasapis, T. C.; Lo, S.-h.; Doak, J. W.; Kim, Y. J.; Wu, C.-I.; Hatzikraniotis, E.; Hogan, T. P.; Seidman, D. N.; Wolverton, C.; Dravid, V. P.; Kanatzidis, M. G. High *zT* in p-Type $(PbTe)_{1-2x}(PbSe)_x(PbS)_x$ Thermoelectric Materials. *J. Am. Chem. Soc.* **2014**, *136*, 3225−3237.

(23) Yamini, S. A.; Wang, H.; Gibbs, Z. M.; Pei, Y.; Dou, S. X.; Snyder, G. J. Chemical Composition Tuning in Quaternary p-type Pb-Chalcogenides - A Promising strategy for Enhanced Thermoelectric Performance. *Phys. Chem. Chem. Phys.* **2014**, *16*, 1835−1840.

(24) Aminorroaya Yamini, S.; Wang, H.; Gibbs, Z. M.; Pei, Y.; Mitchell, D. R. G.; Dou, S. X.; Snyder, G. J. Thermoelectric performance of tellurium-reduced quaternary p-type lead-chalcogenide composites. *Acta Mater.* **2014**, *80*, 365−372.

(25) Yamini, S. A.; Mitchell, D. R. G.; Gibbs, Z. M.; Santos, R.; Patterson, V.; Li, S.; Pei, Y. Z.; Dou, S. X.; Jeffrey Snyder, G. Heterogeneous Distribution of Sodium for High Thermoelectric Performance of p-Type Multiphase Lead-Chalcogenides. *Adv. Energy Mater.* **2015**, *5*, 1501047.

(26) Aminorroaya Yamini, S.; Wang, H.; Ginting, D.; Mitchell, D. R. G.; Dou, S. X.; Snyder, G. J. Thermoelectric Performance of n-Type $(PbTe)_{0.75}(PbS)_{0.15}(PbSe)_{0.1}$ Composites. *ACS Appl. Mater. Interfaces* **2014**, *6*, 11476−11483.

(27) Ginting, D.; Lin, C.-C.; Lydia, R.; So, H. S.; Lee, H.; Hwang, J.; Kim, W.; Al Rahal Al Orabi, R.; Rhyee, J.-S. High Thermoelectric Performance in Pseudo Quaternary Compounds of $(PbTe)_{0.95-x}(PbSe)_x(PbS)_{0.05}$ by Simultaneous Band Convergence and Nano Precipitation. *Acta Mater.* **2017**, *131*, 98−109.

(28) He, J.; Zhao, L.-D.; Zheng, J.-C.; Doak, J. W.; Wu, H.; Wang, H.-Q.; Lee, Y.; Wolverton, C.; Kanatzidis, M. G.; Dravid, V. P. Role of Sodium Doping in Lead Chalcogenide Thermoelectrics. *J. Am. Chem. Soc.* **2013**, *135*, 4624−4627.

(29) Yamini, S. A.; Ikeda, T.; Lalonde, A.; Pei, Y.; Dou, S. X.; Snyder, G. J. Rational design of p-Type Thermoelectric PbTe: Temperature Dependent Sodium Solubility. *J. Mater. Chem. A* **2013**, *1*, 8725−8730.

(30) Aminorroaya Yamini, S.; Patterson, V.; Santos, R. Band-Gap Nonlinearity in Lead Chalcogenide (PbQ, Q = Te, Se, S) alloys. *ACS Omega* **2017**, *2*, 3417−3423.

(31) Ravich, Y. I.; Efimova, B. A.; Smirnov, I. A. *Semiconducting Lead Chalcogenides*; Plenum Press: New York, 1970; pp 196−209.

DOI: 10.1021/acsomega.9b00686
ACS Omega 2019, 4, 9235−9240

(32) Yamini, A.; Li, T.; Mitchell, D. R. G.; Cairney, J. M. Elemental Distributions within Multiphase Quaternary Pb Chalcogenide Thermoelectric Materials Determined through Three-dimensional atom Probe Tomography. *Nano Energy* **2016**, *26*, 157−163.
(33) May, A. F.; Toberer, E. S.; Saramat, A.; Snyder, G. J. Characterization and Analysis of Thermoelectric Transport in n-Type $Ba_8Ga_{16-x}Ge_{30+x}$. *Phys. Rev. B* **2009**, *80*, 125205.
(34) Pei, Y.; LaLonde, A.; Iwanaga, S.; Snyder, G. J. High Thermoelectric Figure of Merit in Heavy Hole Dominated PbTe. *Energy Environ. Sci.* **2011**, *4*, 2085−2089.
(35) Manettas, A.; Santos, R.; Ferreres, X. R.; Aminorroaya Yamini, S. Thermoelectric Performance of Single Phase p-Type Quaternary $(PbTe)_{0.65-x}(PbSe)_{0.35}(PbS)_x$ Alloys. *ACS Appl. Energy Mater.* **2018**, *1*, 1898−1903.
(36) Zhao, L.-D.; He, J.; Wu, C.-I.; Hogan, T. P.; Zhou, X.; Uher, C.; Dravid, V. P.; Kanatzidis, M. G. Thermoelectrics with Earth Abundant Elements: High Performance p-Type PbS Nanostructured with SrS and CaS. *J. Am. Chem. Soc.* **2012**, *134*, 7902−7912.
(37) Pashinkin, A. S.; Mikhailova, M. S.; Malkova, A. S.; Fedorov, V. A. Heat Capacity and Thermodynamic Properties of Lead Selenide and Lead Telluride. *Inorg. Mater.* **2009**, *45*, 1226−1229.
(38) Tobey, B. H. EXPGUI, A Graphical User Interface for GSAS. *J. Appl. Crystallogr.* **2001**, *34*, 210−213.

DOI: 10.1021/acsomega.9b00686
ACS Omega 2019, 4, 9235−9240